A Quadratic-Programming Approach to the Design Optimization of Fractional-Slot Concentrated Windings for Surface Permanent-Magnet Machines

A. Tessarolo, *Senior Member, IEEE*

***Abstract*—Fractional-slot concentrated windings (FSCW) are becoming more and more popular in the design of permanent magnet electric machines. A well-known drawback of their adoption is the occurrence of large magneto-motive force (MMF) harmonics, which produce eddy-current losses in rotor permanent magnets. The use of a multi-layer design, with coils of different phases wound around the same tooth, is a possible countermeasure to mitigate the problem. In this paper, a new general systematic methodology is proposed to optimize the multilayer FSCW design in the form of a multi-objective quadratic programming problem. The maximization of the MMF fundamental and the minimization of total rotor losses are taken as properly weighed objective functions. Constraints are imposed to guarantee the physical feasibility and the electric symmetry of the winding. An application example to a 9-slot 8-pole machine is presented, together with extensive validations by comparison with finite element analysis (FEA) simulations, to prove the effectiveness of the proposed technique.**

***Index Terms*—Concentrated winding, design optimization, eddy current losses, fractional slot, multilayer, quadratic programming, surface permanent magnet.**

I. Introduction

THE use of fractional-slot concentrated windings (FSCW) in the design of permanent magnet synchronous machines is becoming more and more popular [1] thanks to various advantages like improved manufacturability and modularity [2], increased flux weakening performance [3], fault tolerance features [4], reduced end-coil and overall axial length [5]. A well-known drawback of FSCWs is the presence of large magneto-motive force (MMF) space harmonics (especially subharmonics), which cause eddy-current losses in the rotor, with possible consequent overheating and demagnetization issues [6], [7]. Various provisions have been proposed in the literature to reduce FSCW MMF harmonics such as combined star-delta connections among the coils of a phase [8] and use of multi-phase configurations [9]; the most common and promising countermeasure is, however, the adoption of multi-layer arrangements in which more coils, belonging to different phases, are wound around the same tooth [10]–[17]. The simplest form of this design, considered in [11]–[13], is a four-layer winding with two identical coils wound on the same tooth. Through a suitable assignment of the phases to tooth coils, it is possible to reduce or even cancel MMF subharmonics [4], [10], [11]–[13]. However, since 2004 it has been observed that, in a multilayer FSCW, even better results can be achieved if unequal coils, having different number of turns, are employed [14]–[17]. Mostly based on a case-by-case reasoning and through the star-of-slot method [10], it has been proven that suitably selecting the number of turns of the various tooth coils can result in the cancellation of a given MMF harmonic or subharmonic at the expense of a reduction in the MMF fundamental magnitude [15]–[17]. Nevertheless, the question is left unanswered as to whether the proposed solution, identified as "optimal", can be actually further improved through some different arrangement of the tooth coils and a different selection of their number of turns.

This paper presents a new general, systematic and fully-automated approach to the optimization of a three-phase multilayer FSCW for a surface-mounted permanent magnet (SPM) machine, assuming two arbitrarily weighed objectives: maximizing the MMF fundamental on one side and minimizing the total rotor losses (not a specific MMF harmonic) on the other. Constraints are imposed to guarantee that the winding is feasible using (non-overlapping) tooth coils [4] and is electrically symmetric. The optimization is formulated as a dual-objective quadratic programming problem subject to linear constraints, which can easily be solved using existing computationally-efficient algorithms [18].

The paper is organized as follows. In Section II, the model of a multilayer FSCW is introduced and its air-gap MMF harmonics are analyzed. In Section III, an analytical model is described to compute magnet eddy-current losses produced by MMF harmonics. Section IV defines the optimal design of the FSCW in the form of a multi-objective quadratic programming problem. Section V presents an example of solution and validates the design optimization procedure through FEA simulations.

II. Multilayer FSCW Model and MMF Analysis

A. Multilayer FSCW Model

For a multilayer FSCW machine, each of the Z stator teeth is assumed to have the structure shown in Fig. 1(a). In general, three coils are wound around it, one for each of the three phases a, b and c. Choosing a conventional positive direction for the

Manuscript received June 20, 2017; accepted September 5, 2017. Date of publication September 12, 2017; date of current version February 16, 2018. Paper no. TEC-00466-2017.

The author is with the Engineering and Architecture Department of the University of Trieste, Trieste 34127, Italy (e-mail: atessarolo@units.it).

Color versions of one or more of the figures in this paper are available online at http://ieeexplore.ieee.org.

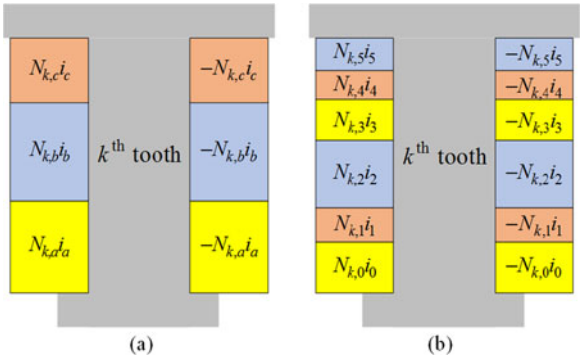

Fig. 1. (a) Phase sub-coils wound on the kth turn are relevant amperturns; (b) Equivalent configuration with six sub-coils per tooth.

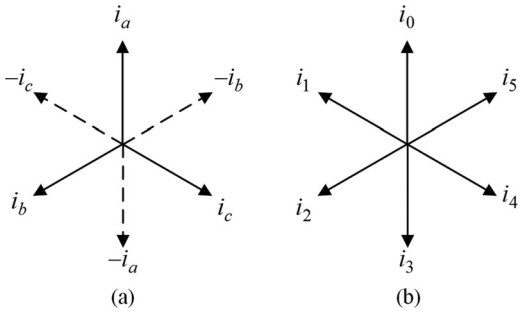

Fig. 2. (a) Phase current phasors. (b) Equivalent sub-phase phasors.

current (e.g., positive if entering the page, negative otherwise), the numbers of turns $N_{k,a}$, $N_{k,b}$ and $N_{k,c}$ of the three coils must be taken positive or negative depending on the direction of the relevant currents i_a, i_b and i_c. Hence, calling N_0 the total number of turns which can be wound around a tooth, the following constraint must hold:

$$|N_{k,a}| + |N_{k,b}| + |N_{k,c}| \leq N_0 \tag{1}$$

and the total amperturns flowing around the kth tooth are:

$$N_{k,a}i_a + N_{k,b}i_b + N_{k,c}i_c. \tag{2}$$

Regardless of the objective function, the FSCW optimal design implies determining the number of turns $N_{k,a}$, $N_{k,b}$ and $N_{k,c}$ (design variables) for any $k = 0, 1, \ldots, Z-1$ under suitable constraints, including (1).

The optimization approach proposed in this paper, based on quadratic programming, can be applied if the objective function is a linear or quadratic function of the design variables [18]. Moreover, it requires the constraints to be linear equalities or inequalities. Therefore, (1) is unfit as a constraint due to its intrinsic non-linear nature with respect to the design variables $N_{k,a}$, $N_{k,b}$ and $N_{k,c}$. To get round the problem, it is convenient to introduce a system of fictitious "sub-currents" i_0, i_1, i_3, i_4, i_5, whose phasors are shown in Fig. 2 together with the phasors of the physical currents i_a, i_b and i_c. It is easily seen that

$$i_a = i_0 = -i_3,\ i_b = i_2 = -i_5,\ i_c = i_4 = -i_1. \tag{3}$$

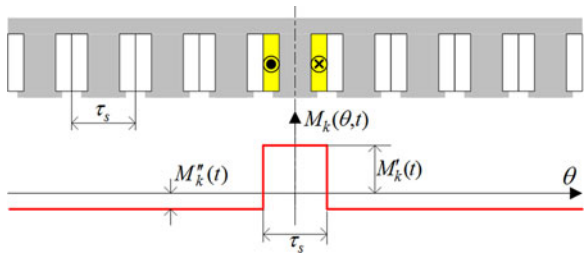

Fig. 3. Air-gap MMF produced by the kth wound tooth energized with a total current $i_k(t)$.

With such a choice, each phase coil wound on the kth tooth can be split into a couple of "sub-coils" having the same overall number of turns, as shown in Fig. 1(b). As a result, six sub-coils are wound around the tooth, each composed of $N_{k,j} \geq 0$ turns with $j = 0, 1, \ldots, 5$, such that

$$N_{k,0} + N_{k,1} + N_{k,2} + N_{k,3} + N_{k,4} + N_{k,5} \leq N_0. \tag{4}$$

The amperturns flowing around the kth tooth are now:

$$N_{k,0}i_0 + N_{k,1}i_1 + N_{k,2}i_2 + N_{k,3}i_3 + N_{k,4}i_4 + N_{k,5}i_5. \tag{5}$$

For the configurations depicted in Fig. 1(a) and Fig. 1(b) to be equivalent in terms of air-gap MMF, we must impose that (2) and (5) be equal. Based on (3), this happens if:

$$\begin{aligned} &N_{k,a} = N_{k,0} - N_{k,3}, \\ &N_{k,b} = N_{k,2} - N_{k,5},\ N_{k,c} = N_{k,4} - N_{k,1}. \end{aligned} \tag{6}$$

The model assumed in the rest of the paper is therefore that shown in Fig. 1(b), which is equivalent to the physical configuration (Fig. 1(a)) under the assumption (6). Accordingly, the design variables will be the positive or null quantities $N_{k,j}$ subject to the linear constraint (4). Taking the phase "a" (or sub-phase "0") as a reference, the currents flowing in the six sub-coils of each tooth will be:

$$i_j(t) = I_0 \cos\left(\omega t - \frac{\pi}{3}j\right), \tag{7}$$

where I_0 and f are the phase current amplitude and frequency, $\omega = 2\pi f$ and $j = 0, 1, \ldots, 5$.

B. Air-Gap MMF Harmonic Computation

In order to optimize the FSCW design with respect to its space harmonic content, it is necessary to derive an explicit expression for the air-gap MMF harmonics as functions of the design variables identified in the previous subsection, i.e., the numbers of turns $N_{k,j}$.

In the hypothesis of unsaturated stator and rotor cores, the air-gap MMF due to the entire winding can be computed by summing the contributions of each tooth. For the kth tooth, the air-gap MMF $M_k(\theta, t)$ due to its amperturns (5) has the waveform shown in Fig. 3, where $\tau_s = 2\pi/Z$ and [19]:

$$M'_k(t) = \frac{Z-1}{Z}\sum_{j=0..5} N_{k,j}i_j(t),\ M''_k(t) = \frac{-1}{Z}\sum_{j=0..5} N_{k,j}i_j(t). \tag{8}$$

Using Fourier series, the expression for $M_k(\theta,\, t)$ is [19]:

$$M_k(\theta,t)=\left(\sum_{j=0..5} N_{k,j}\, i_k(t)\right)\left(\sum_{n=1..\infty} a_n \cos\left(n\theta\right)\right) \quad (9)$$

with a_n given by:

$$a_n=\frac{2}{\pi}\frac{1}{n}(-1)^n \sin\left(\frac{\pi\, n\,(Z-1)}{Z}\right). \quad (10)$$

Summing over all the teeth (displaced by $2\pi/Z$ apart) and substituting (8), the total air-gap MMF is:

$$M(\theta,t)=\sum_{k=0..Z-1} M_k\left(\theta-k\frac{2\pi}{Z},t\right)=\sum_{k=0..Z-1}\sum_{j=0..5}\sum_{n=1..\infty} a_n N_{k,j} I_0 \cos\left(\omega t-j\frac{\pi}{3}\right)\cos\left(n\theta-nk\frac{2\pi}{Z}\right) \quad (11)$$

Equation (11) can be manipulated using the identity

$$\cos\left(\omega t-j\frac{\pi}{3}\right)\cos\left(n\theta-nk\frac{2\pi}{Z}\right) = \mathrm{Re}\left\{e^{i\left(\omega t-j\frac{\pi}{3}\right)}\frac{1}{2}\left[e^{i\left(n\theta-nk\frac{2\pi}{Z}\right)}+e^{-i\left(n\theta-nk\frac{2\pi}{Z}\right)}\right]\right\} \quad (12)$$

and, after few passages, can be put in the following form:

$$\begin{aligned} M(\theta,t) &= \mathrm{Re}\left\{\sum_{n=1..\infty}\left[m_n^- e^{i(\omega t-n\theta)}+m_n^+ e^{i(\omega t+n\theta)}\right]\right\} \\ &= \mathrm{Re}\left\{\sum_{n=1..\infty}\left[\left|m_n^-\right| e^{i(\omega t-n\theta+\arg(m_n^-))}\right.\right. \\ &\quad \left.\left.+\left|m_n^+\right| e^{i\left(\omega t+n\theta+\arg(m_n^+)\right)}\right]\right\} \\ &= \sum_{n=1..\infty}\left[\left|m_n^-\right|\cos\left[\omega t-n\theta+\arg\left(m_n^-\right)\right]\right. \\ &\quad \left.+\left|m_n^+\right|\cos\left[\omega t+n\theta+\arg\left(m_n^+\right)\right]\right] \end{aligned} \quad (13)$$

where

$$m_n^-=\frac{a_n I_0}{2}\sum_{k=0..Z-1}\sum_{j=0..5} N_{k,j} e^{i\left(-\frac{\pi}{3}j+kn\frac{2\pi}{Z}\right)} \quad (14)$$

$$m_n^+=\frac{a_n I_0}{2}\sum_{k=0..Z-1}\sum_{j=0..5} N_{k,j} e^{i\left(-\frac{\pi}{3}j-kn\frac{2\pi}{Z}\right)} \quad (15)$$

are the complex coefficients for the $n\mathrm{th}-\mathrm{order}$ MMF space harmonics respectively revolving in the same (sign "−") and opposite (sign "+") direction with respect to the rotor.

A more compact expression for (14), (15) can be obtained if all the variables $N_{k,j}$ are grouped into a single 6*Z*-sized "turn vector" **x** defined as follows:

$$\mathbf{x}=\left(N_{0,0}\cdots N_{1,5}\mid N_{1,0}\cdots N_{1,5}\mid\cdots\mid N_{Z-1,0}\cdots N_{Z-1,5}\right)^T, \quad (16)$$

such that

$$[\mathbf{x}]_{6k+j}=N_{k,j}\quad \forall j=0..5,\ k=0..Z-1. \quad (17)$$

This allows for (14), (15) to be written as:

$$\begin{aligned} m_n^{\pm} &= \frac{a_n I_0}{2}\sum_{h=0..6Z-1}[\mathbf{x}]_h e^{i\left[-\frac{\pi}{3}\ \mathrm{mod}\ (h,6)\mp n\frac{2\pi}{Z}\mathrm{floor}(h/6)\right]} \\ &= \mathbf{v}_n^{\pm T}\mathbf{x} \end{aligned} \quad (18)$$

where mod(*x*, *y*) and floor(*x*, *y*) respectively return the reminder and integer part for the division of *x* by *y* and the complex vectors $\mathbf{v}_n^+$ and $\mathbf{v}_n^-$ are defined as follows:

$$\left[\mathbf{v}_n^{\pm}\right]_h=\frac{1}{2}a_n I_0 e^{i\left[-\frac{\pi}{3}\ \mathrm{mod}\ (h,6)\mp n\frac{2\pi}{Z}\mathrm{floor}(h,6)\right]}\ \forall h=0..6Z-1 \quad (19)$$

Based on (18), the air-gap space harmonic amplitudes appearing in (13) can be then expressed as:

$$\begin{aligned} \left|m_n^{\pm}\right| &= \sqrt{\bar{m}_n^{\pm} m_n^{\pm}}=\sqrt{\overline{\left(\mathbf{v}_n^{\pm T}\mathbf{x}\right)}\left(\mathbf{v}_n^{\pm T}\mathbf{x}\right)} \\ &= \sqrt{\overline{\left(\mathbf{v}_n^{\pm T}\mathbf{x}\right)}^T\left(\mathbf{v}_n^{\pm T}\mathbf{x}\right)}=\sqrt{\mathbf{x}^T\bar{\mathbf{v}}_n^{\pm}\mathbf{v}_n^{\pm T}\mathbf{x}}=\sqrt{\mathbf{x}^T\mathbf{H}_n^{\pm}\mathbf{x}} \end{aligned} \quad (20)$$

where overlines indicate complex conjugates and $\mathbf{H}_n^{\pm}$ are the symmetric $6Z\times 6Z$ matrices defined as follows:

$$\mathbf{H}_n^{\pm}=\bar{\mathbf{v}}_n^{\pm}\mathbf{v}_n^{\pm T}. \quad (21)$$

According to this definition, $\mathbf{H}_n^{\pm}$ are complex-valued matrices. However, we observe that, being the **x** vector (16) real, from (20) one can write:

$$\left|m_n^{\pm}\right|^2=\mathrm{Re}\left\{\left|m_n^{\pm}\right|^2\right\}=\mathbf{x}^T\,\mathrm{Re}\left\{\mathbf{H}_n^{\pm}\right\}\mathbf{x}=\mathbf{x}^T\mathbf{Q}_n^{\pm}\mathbf{x}, \quad (22)$$

where $\mathbf{Q}_n^{\pm}=\mathrm{Re}\{\mathbf{H}_n^{\pm}\}$ are real-valued symmetric matrices. Based on (21), they can be computed as:

$$\begin{aligned} \mathbf{Q}_n^{\pm} &= \mathrm{Re}\left\{\bar{\mathbf{v}}_n^{\pm}\mathbf{v}_n^{\pm T}\right\} \\ &= \mathrm{Re}\left\{\mathbf{v}_n^{\pm}\right\}\mathrm{Re}\left\{\mathbf{v}_n^{\pm T}\right\}+\mathrm{Im}\left\{\mathbf{v}_n^{\pm}\right\}\mathrm{Im}\left\{\mathbf{v}_n^{\pm T}\right\} \end{aligned} \quad (23)$$

C. Single Phase Contribution to the MMF Fundamental

One of the constraints to be imposed for the FSCW optimization will be the symmetry of the three-phase system. In order to formalize this constraint, it is useful to identify the contribution of the three phases to the MMF fundamental. The latter is obtained from (13) considering only the harmonic order *n* equal to the number of pole pairs *p* and revolving in the same direction as the rotor, that is:

$$M_{fund}(\theta,t)=\mathrm{Re}\left\{m_p^- e^{i(\omega t-p\theta)}\right\}. \quad (24)$$

Substitution of (18) into (24) gives:

$$M_{fund}(\theta,t)=\mathrm{Re}\left\{\mathbf{v}_p^{-T}\mathbf{x}e^{i(\omega t-p\theta)}\right\}. \quad (25)$$

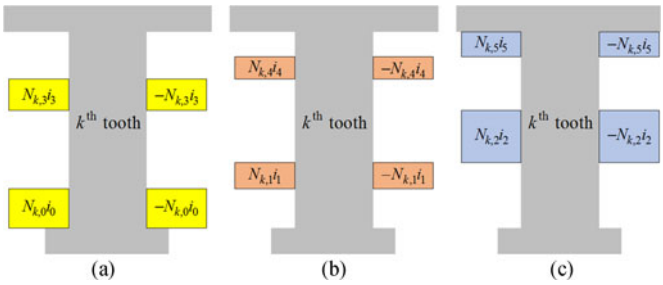

Fig. 4. kth wound tooth configuration when the turn vector is equal to (a) $\mathbf{x}_a = \mathbf{K}_a\mathbf{x}$; (b) $\mathbf{x}_b = \mathbf{K}_b\mathbf{x}$; (c) $\mathbf{x}_c = \mathbf{K}_c\mathbf{x}$.

To determine the MMF fundamentals due to the three phases individually, we introduce the following 6×6 matrices:

$$\mathbf{K}_{6a} = \begin{pmatrix} 1&0&0&0&0&0\\ 0&0&0&0&0&0\\ 0&0&0&0&0&0\\ 0&0&0&1&0&0\\ 0&0&0&0&0&0\\ 0&0&0&0&0&0 \end{pmatrix}, \mathbf{K}_{6b} = \begin{pmatrix} 0&0&0&0&0&0\\ 0&1&0&0&0&0\\ 0&0&0&0&0&0\\ 0&0&0&0&0&0\\ 0&0&0&0&1&0\\ 0&0&0&0&0&0 \end{pmatrix},$$
$$\mathbf{K}_{6c} = \begin{pmatrix} 0&0&0&0&0&0\\ 0&0&0&0&0&0\\ 0&0&1&0&0&0\\ 0&0&0&0&0&0\\ 0&0&0&0&0&0\\ 0&0&0&0&0&1 \end{pmatrix}, \mathbf{0}_6 = \begin{pmatrix} 0&0&0&0&0&0\\ 0&0&0&0&0&0\\ 0&0&0&0&0&0\\ 0&0&0&0&0&0\\ 0&0&0&0&0&0\\ 0&0&0&0&0&0 \end{pmatrix}, \tag{26}$$

and use them to build the following $6Z \times 6Z$ matrices:

$$\mathbf{K}_a = \begin{pmatrix} \mathbf{K}_{6a} & \mathbf{0}_6 & \cdots & \mathbf{0}_6 \\ \mathbf{0}_{6a} & \mathbf{K}_{6a} & \cdots & \mathbf{0}_6 \\ \vdots & \vdots & \ddots & \vdots \\ \mathbf{0}_6 & \mathbf{0}_6 & \cdots & \mathbf{K}_{6a} \end{pmatrix}, \mathbf{K}_b = \begin{pmatrix} \mathbf{K}_{6b} & \mathbf{0}_6 & \cdots & \mathbf{0}_6 \\ \mathbf{0}_6 & \mathbf{K}_{6b} & \cdots & \mathbf{0}_6 \\ \vdots & \vdots & \ddots & \vdots \\ \mathbf{0}_6 & \mathbf{0}_6 & \cdots & \mathbf{K}_{6b} \end{pmatrix},$$
$$\mathbf{K}_c = \begin{pmatrix} \mathbf{K}_{6c} & \mathbf{0}_6 & \cdots & \mathbf{0}_6 \\ \mathbf{0}_6 & \mathbf{K}_{6c} & \cdots & \mathbf{0}_6 \\ \vdots & \vdots & \ddots & \vdots \\ \mathbf{0}_6 & \mathbf{0}_6 & \cdots & \mathbf{K}_{6c} \end{pmatrix}. \tag{27}$$

It can be easily seen that, when summed together, the matrices in (27) give the $6Z \times 6Z$ identity matrix $\mathbf{I}_{6Z}$. Hence, the turn vector $\mathbf{x}$ can be also written as:

$$\mathbf{x} = \mathbf{I}_{6Z}\mathbf{x} = (\mathbf{K}_a + \mathbf{K}_b + \mathbf{K}_c)\,\mathbf{x} = \mathbf{x}_a + \mathbf{x}_b + \mathbf{x}_c \tag{28}$$

where

$$\mathbf{x}_a = \mathbf{K}_a\mathbf{x},\ \mathbf{x}_b = \mathbf{K}_b\mathbf{x},\ \mathbf{x}_c = \mathbf{K}_c\mathbf{x}. \tag{29}$$

Considering the structure of $\mathbf{K}_a$ and of the turn vector $\mathbf{x}$, it is apparent that $\mathbf{x}_a$ represent a new FSCW where the number of turns for sub-phases "0" and "3" (corresponding to "a" and "$-a$", Fig. 2) is the same as in $\mathbf{x}$ while all the other sub-phases are set to have zero turns. As an example, the winding configuration identified by the turn vector $\mathbf{x}_a$ is shown in Fig. 4(a) for the kth tooth. Similarly, Figs. 4(b) and 4(c) show the winding configurations identified by the turn vectors $\mathbf{x}_b$ and $\mathbf{x}_c$, where only the turns of phases "b" and "c" are considered, respectively.

Substitution of (28) into (25) gives:

$$\begin{aligned} M_{fund}(\theta,t) &= \mathrm{Re}\left\{\mathbf{v}_p^{-T}\left(\mathbf{x}_a + \mathbf{x}_b + \mathbf{x}_c\right)e^{i(\omega t - p\theta)}\right\} \\ &= M_{fund,a}(\theta,t) + M_{fund,b}(\theta,t) + M_{fund,c}(\theta,t), \end{aligned} \tag{30}$$

where $M_{fund,a}$, $M_{fund,b}$ and $M_{fund,c}$ are:

$$\begin{aligned} M_{fund,a}(\theta,t) &= \mathrm{Re}\left\{\mathbf{v}_p^{-T}\mathbf{x}_a e^{i(\omega t - p\theta)}\right\} \\ &= \left|\mathbf{v}_p^{-}\mathbf{x}_a{}^T\right|\cos\left(\omega t - p\theta + \arg(\mathbf{v}_p^{-T}\mathbf{x}_a)\right), \end{aligned} \tag{31}$$

$$\begin{aligned} M_{fund,b}(\theta,t) &= \mathrm{Re}\left\{\mathbf{v}_p^{-T}\mathbf{x}_b e^{i(\omega t - p\theta)}\right\} \\ &= \left|\mathbf{v}_p^{-T}\mathbf{x}_b\right|\cos\left(\omega t - p\theta + \arg(\mathbf{v}_p^{-T}\mathbf{x}_b)\right), \end{aligned} \tag{32}$$

$$\begin{aligned} M_{fund,c}(\theta,t) &= \mathrm{Re}\left\{\mathbf{v}_p^{-T}\mathbf{x}_c e^{i(\omega t - p\theta)}\right\} \\ &= \left|\mathbf{v}_p^{-T}\mathbf{x}_c\right|\cos\left(\omega t - p\theta + \arg(\mathbf{v}_p^{-T}\mathbf{x}_c)\right) \end{aligned} \tag{33}$$

and represent the MMF fundamentals produced by the three phases a, b and c individually.

In order for the winding to be symmetric, the three sinusoidal waves in (31)–(33) must be equal in magnitude and phase, which implies the equality of the three complex numbers $\mathbf{v}_p^{-T}\mathbf{x}_a$, $\mathbf{v}_p^{-T}\mathbf{x}_b$ and $\mathbf{v}_p^{-T}\mathbf{x}_c$, i.e.,:

$$\begin{aligned} \mathrm{Re}\left\{v_p^{-T}\left(\mathbf{x}_b - \mathbf{x}_a\right)\right\} &= \mathrm{Im}\left\{v_p^{-T}\left(\mathbf{x}_b - \mathbf{x}_a\right)\right\} = 0, \\ \mathrm{Re}\left\{v_p^{-T}\left(\mathbf{x}_c - \mathbf{x}_b\right)\right\} &= \mathrm{Im}\left\{v_p^{-T}\left(\mathbf{x}_c - \mathbf{x}_b\right)\right\} = 0, \end{aligned} \tag{34}$$

Considering (29), this results in the following set of linear constraints to be applied to the turn vector $\mathbf{x}$:

$$\begin{aligned} \mathrm{Re}\left\{v_p^{-T}\left(\mathbf{K}_b - \mathbf{K}_a\right)\right\}\mathbf{x} &= \mathrm{Im}\left\{v_p^{-T}\left(\mathbf{K}_b - \mathbf{K}_a\right)\right\}\mathbf{x} = 0 \\ \mathrm{Re}\left\{v_p^{-T}\left(\mathbf{K}_c - \mathbf{K}_b\right)\right\}\mathbf{x} &= \mathrm{Im}\left\{v_p^{-T}\left(\mathbf{K}_c - \mathbf{K}_b\right)\right\}\mathbf{x} = 0 \end{aligned} \tag{35}$$

III. Calculation of Magnet Eddy-Current Losses

One of the objectives of the FSCW optimization is reducing the eddy-current losses which arise in the magnets as a consequence of the air-gap MMF harmonics analyzed in II.*B*. To this end, it is important to have a fast but accurate formula that expresses the eddy-current losses produced in the magnets by each of the stator MMF space harmonic. In the literature, the problem has been often addressed through conformal transformations leading to a linear geometry for the air-gap [6]. However, the use of conformal transformations for energy or loss computation can introduce some inaccuracies [20]. For this reason, it is found safer to consider a circular air-gap model like that shown in Fig. 5 as described next.

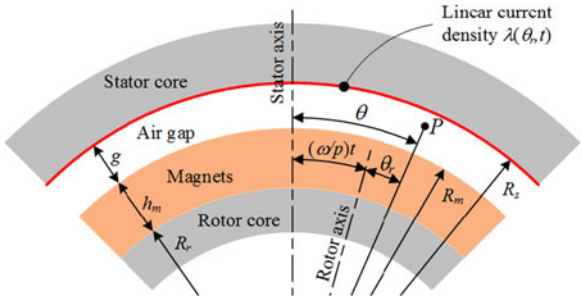

Fig. 5. Geometric model for the analysis of magnet eddy-current losses due to air-gap MMF harmonics.

A. Model for Magnet Loss Computation

With regard to Fig. 5, the following simplifications are assumed: stator slotting is neglected; stator and rotor cores are assumed infinitely permeable; rotor magnets are modeled as a continuous annulus with magnetic permeability μ and electric conductivity σ. Introducing a rotor-attached polar reference frame with coordinates r and θ_r (which revolves at ω/p radians per second) and calling θ the angular position of a generic point P in the stator reference frame, its position θ_r with respect to the rotor is such that

$$\theta = \theta_r + \frac{\omega}{p}t. \tag{36}$$

Substitution of (36) into (13) leads to express the stator MMF in rotor coordinates as follows:

$$M\left(\theta_r + \frac{\omega}{p}t, t\right) = \mathrm{Re}\left\{\sum_{n=1..\infty}\left[m_n^- e^{i\left(\omega\left(1-\frac{n}{p}\right)t - n\theta_r\right)} + m_n^+ e^{i\left(\omega\left(1+\frac{n}{p}\right)t + n\theta_r\right)}\right]\right\} \tag{37}$$

In the model shown in Fig. 5, stator MMF is represented by an equivalent linear current distribution $\lambda(\theta_r, t)$, spread around the stator bore surface, such that [19]:

$$\lambda(\theta_r, t) = \frac{1}{R_s}\frac{\partial}{\partial\theta_r}M\left(\theta_r + \frac{\omega}{p}t, t\right), \tag{38}$$

This naturally imposes a tangential component of the air-gap magnetic field at $r = R_s$ given by:

$$\begin{aligned} H_\theta(\theta_r, t)|_{r=R_s} &= \lambda(\theta_r, t) \\ &= \frac{1}{R_s}\mathrm{Re}\left\{\sum_{n=1..\infty}\left[-n\, m_n^- e^{i\left(\omega\left(1-\frac{n}{p}\right)t - n\theta_r\right)} + n\, m_n^+ e^{i\left(\omega\left(1+\frac{n}{p}\right)t + n\theta_r\right)}\right]\right\} \end{aligned} \tag{39}$$

Such magnetic field can be expressed by the following complex phasors (functions of θ_r):

$$H_\theta^\pm(\theta_r)\big|_{r=R_s} = \pm\frac{1}{R_s}\sum_{n=1..\infty} n\, m_n^\pm e^{\pm in\theta_r}, \tag{40}$$

associated to the rotor frequencies:

$$\omega_n^\pm = \omega(1 \pm n/p). \tag{41}$$

B. Determining the Vector Potential in the Magnet Region

Given the generic $n\mathrm{th}-\mathrm{order}$ harmonic, associated to the rotor frequency $\omega_n^\pm$, we shall call $U_n^\pm(\theta_r, r)$ and $V_n^\pm(\theta_r, r)$ the complex vector potentials it produces respectively in the gap and magnet regions. The two vector potentials obey to the following Laplace's and Helmholtz's differential equations [21]:

$$\frac{\partial^2 U_n^\pm}{\partial r^2} + \frac{1}{r}\frac{\partial U_n^\pm}{\partial r} + \frac{1}{r^2}\frac{\partial^2 U_n^\pm}{\partial {\theta_r}^2} = 0,\ R_m \le r \le R_s \tag{42}$$

$$\frac{\partial^2 V_n^\pm}{\partial r^2} + \frac{1}{r}\frac{\partial V_n^\pm}{\partial r} + \frac{1}{r^2}\frac{\partial^2 V_n^\pm}{\partial {\theta_r}^2} = i\omega_n^\pm\mu\sigma V_n^\pm,\ R_r \le r < R_m \tag{43}$$

where R_r, R_m and R_s are the radii shown in Fig. 5. The general solution for (42), (43) is assumed in the form below [21]:

$$U_n^\pm(r, \theta_r) = \left(A_n^\pm r^n + B_n^\pm r^{-n}\right)e^{\pm in\theta_r}, \tag{44}$$

$$V_n^\pm(r, \theta_r) = \left[C_n^\pm J_n\left(\kappa_n^\pm r\right) + D_n^\pm Y_n\left(\kappa_n^\pm r\right)\right]e^{\pm in\theta_r}, \tag{45}$$

where: $J_n(\cdot)$ and $Y_n(\cdot)$ are the $n\mathrm{th}-\mathrm{order}$ Bessel functions of the first and second kind; $A_n^\pm$, $B_n^\pm$, $C_n^\pm$ and $D_n^\pm$ are complex coefficients depending on boundary conditions; $\kappa_n^\pm$ is a complex coefficient such that $(\kappa_n^\pm)^2 = -i\sigma\mu\omega_n^\pm$, i.e.,:

$$\kappa_n^\pm = \sqrt{-i\sigma\mu\omega_n^\pm} = (1-i)\sqrt{\sigma\mu\omega_n^\pm/2}. \tag{46}$$

To determine coefficients $A_n^\pm$, $B_n^\pm$, $C_n^\pm$ and $D_n^\pm$, the following boundary conditions are established:

$$\pm\frac{1}{R_s}n\, m_n^\pm e^{\pm in\theta_r} = -\frac{1}{\mu_0}\frac{\partial U_n^\pm}{\partial r}\bigg|_{r=R_s}, \tag{47}$$

$$\frac{\partial U_n^\pm}{\partial\theta_r}\bigg|_{r=R_m} = \frac{\partial V_n^\pm}{\partial\theta_r}\bigg|_{r=R_m},\ \frac{\partial U_n^\pm}{\partial r}\bigg|_{r=R_m} = \frac{\partial V_n^\pm}{\partial r}\bigg|_{r=R_m}, \tag{48}$$

$$\frac{\partial V_n^\pm}{\partial r}\bigg|_{r=R_r} = 0, \tag{49}$$

where: (47) imposes that the magnetic field tangential component at $r = R_s$ be equal to that given by (40); equations (48) impose the continuity of the radial and tangential field components across the boundary ($r = R_m$) between the gap and the magnets; (49) imposes that the magnetic field be purely radial on $r = R_r$. Equations (47)–(49), after the substitution of (44), (45), result in a linear system from which the coefficients $C_n^\pm$ and $D_n^\pm$ can be determined as follows:

$$C_n^\pm = -\frac{2i\mu_0 n\varphi_n^\pm m_n^\pm}{\Delta_n^\pm R_s {R_m}^2},\ D_n^\pm = \frac{2i\mu_0 n\varepsilon_n^\pm m_n^\pm}{\Delta_n^\pm R_s {R_m}^2}, \tag{50}$$

where $\varepsilon_n^\pm$, $\varphi_n^\pm$ and $\Delta_n^\pm$ are defined by (51)–(56):

$$\begin{aligned} \Delta_n^\pm = &\left(\beta_n^\pm\varepsilon_n^\pm - \alpha_n^\pm\varphi_n^\pm - i\delta_n^\pm\varepsilon_n^\pm + i\chi_n^\pm\varphi_n^\pm\right){R_s}^{n-1}{R_m}^{-n-1} \\ &+ \left(\alpha_n^\pm\varphi_n^\pm - \beta_n^\pm\varepsilon_n^\pm - i\delta_n^\pm\varepsilon_n^\pm + i\chi_n^\pm\varphi_n^\pm\right){R_m}^{n-1}{R_s}^{-n-1} \end{aligned} \tag{51}$$

$$\alpha_n^\pm = i\,n\,J_n\left(\kappa_n^\pm R_m\right){R_m}^{-1},\ \beta_n^\pm = -i\,n\,Y_n\left(\kappa_n^\pm R_m\right){R_m}^{-1}, \tag{52}$$

$$\chi_n^\pm = -\kappa_n^\pm J_{n+1}\left(\kappa_n^\pm R_m\right) + n\,{R_m}^{-1}J_n\left(\kappa_n^\pm R_m\right), \tag{53}$$

$$\delta_n^{\pm} = -\kappa_n^{\pm} Y_{n+1}\left(\kappa_n^{\pm} R_m\right) + n\, {R_m}^{-1}\, Y_n\left(\kappa_n^{\pm} R_m\right), \quad (54)$$

$$\varepsilon_n^{\pm} = \kappa_n^{\pm} J_{n+1}\left(\kappa_n^{\pm} R_r\right) - n\, {R_r}^{-1} J_n\left(\kappa_n^{\pm} R_r\right) \quad (55)$$

$$\varphi_n^{\pm} = \kappa_n^{\pm} Y_{n+1}\left(\kappa_n^{\pm} R_r\right) - n\, {R_r}^{-1} Y_n\left(\kappa_n^{\pm} R_r\right) \quad (56)$$

C. Determining Magnet Losses

Once the vector potential (45) in the magnet region is evaluated through (50)–(56), the eddy current density phasor $j_n^{\pm}$ in the magnets due to the $n\text{th}-\text{order}$ harmonic is also known as [21]:

$$j_n^{\pm}(r,\theta_r) = -i\omega_n^{\pm}\sigma V_n^{\pm}(r,\theta_r). \quad (57)$$

The eddy current losses $P_n^{\pm}$ in the magnet region due to the $n\text{th}-\text{order}$ harmonic will then be [21]:

$$\begin{aligned} P_n^{\pm} &= \frac{L}{2\sigma}\int_0^{2\pi}\int_{R_r}^{R_m} \left|j_n^{\pm}(r,\theta_r)\right|^2 r\, dr d\theta_r \\ &= \pi\, L\omega_n^{\pm 2}\sigma \int_{R_r}^{R_m} \left|C_n^{\pm} J_n\left(\kappa_n^{\pm} r\right) + D_n^{\pm} Y_n\left(\kappa_n^{\pm} r\right)\right|^2 r\, dr \end{aligned} \quad (58)$$

where L is the machine axial length. By substituting (50) into (58), one obtains:

$$\begin{aligned} P_n^{\pm} &= \frac{4\pi {\mu_0}^2 n^2 L \omega_n^{\pm 2}\sigma}{{R_m}^4 {R_s}^2 \left|\Delta_n^{\pm}\right|^2}\left|m_n^{\pm}\right|^2 \\ &\times \int_{R_r}^{R_m} \left|\varepsilon_n^{\pm} Y_n\left(\kappa_n^{\pm} r\right) - \varphi_n^{\pm} J_n\left(\kappa_n^{\pm} r\right)\right|^2 r\, dr = p_n^{\pm}\left|m_n^{\pm}\right|^2 \end{aligned} \quad (59)$$

where $p_n^{\pm}$ gives the losses due to the $n\text{th}-\text{order}$ MMF harmonic, associated to the rotor frequency $\omega_n^{\pm}$ and having a unit magnitude, i.e.,:

$$p_n^{\pm} = \frac{4\pi {\mu_0}^2 n^2 L \omega_n^{\pm 2}\sigma}{{R_m}^4 {R_s}^2 \left|\Delta_n^{\pm}\right|^2}\int_{R_r}^{R_m} \left|\varepsilon_n^{\pm} Y_n\left(\kappa_n^{\pm} r\right) - \varphi_n^{\pm} J_n\left(\kappa_n^{\pm} r\right)\right|^2 r\, dr. \quad (60)$$

It is known that the superposition principle can be applied to the losses caused by different MMF harmonics [22]. Therefore, the total losses P_{loss} in the magnets are

$$P_{loss} = \sum_{n=1..\infty}\left(P_n^{+} + P_n^{-}\right) = \sum_{n=1..\infty}\left(p_n^{+}\left|m_n^{+}\right|^2 + p_n^{-}\left|m_n^{-}\right|^2\right) \quad (61)$$

and, using (22), they can be written as:

$$\begin{aligned} P_{loss} &= \sum_{n=1..\infty}\left(p_n^{+}\mathbf{x}^T\mathbf{Q}_n^{+}\mathbf{x} + p_n^{-}\mathbf{x}^T\mathbf{Q}_n^{-}\mathbf{x}\right). \\ &= \mathbf{x}^T\left[\sum_{n=1..\infty}\left(p_n^{+}\mathbf{Q}_n^{+} + p_n^{-}\mathbf{Q}_n^{-}\right)\right]\mathbf{x} \end{aligned} \quad (62)$$

The total magnet losses are thus expressed as a quadratic function of the turn vector $\mathbf{x}$.

IV. Quadratic Programming Problem Formulation

At this point of the treatment, we have all the equations ready to define the FSCW optimal design as a quadratic programming problem. For this purpose, we shall separately identify the objective function and the constraints.

A. Objective Function

The optimal design of the multilayer FSCW is, intrinsically, a dual-objective optimization problem: one objective is maximizing the MMF fundamental (or, equivalently, the winding factor); the other is to minimize rotor losses due to MMF space harmonics. In more formal terms, we can introduce the two objective functions below:

$$f_{fund}(\mathbf{x}) = -\left|m_p^{-}\right|^2 = -\mathbf{x}^T\mathbf{Q}_p\mathbf{x}, \quad (63)$$

$$f_{loss}(\mathbf{x}) = \mathbf{x}^T\left[\sum_{n=1..\infty}\left(p_n^{+}\mathbf{Q}_n^{+} + p_n^{-}\mathbf{Q}_n^{-}\right)\right]\mathbf{x}. \quad (64)$$

The former returns minus the square of the magnitude of the MMF fundamental based on (22); the latter returns the total magnet losses due to MMF harmonics based on (62). Both functions are to be minimized.

An effective way to cope with dual-objective optimization problems is it to simplify them into a single-objective form though a weighed sum. For example, we can define a weighing coefficient $w \in [0, 1]$ and generate the following w-dependent objective function:

$$f_w(\mathbf{x}) = (1-w)\, f_{fund}(\mathbf{x}) + w\, f_{loss}(\mathbf{x}) =$$

$$\mathbf{x}^T\left[-(1-w)\,\mathbf{Q}_p^{-} + w\sum_{n=1..\infty}\left(p_n^{+}\mathbf{Q}_n^{+} + p_n^{-}\mathbf{Q}_n^{-}\right)\right]\mathbf{x} = \mathbf{x}^T\mathbf{F}_w\mathbf{x}, \quad (65)$$

where the $6Z \times 6Z$ real symmetric matrix $\mathbf{F}_w$ is given by:

$$\mathbf{F}_w = (w-1)\,\mathbf{Q}_p^{-} + w\sum_{n=1..\infty}\left(p_n^{+}\mathbf{Q}_n^{+} + p_n^{-}\mathbf{Q}_n^{-}\right). \quad (66)$$

Equation (65) therefore defines the total quantity to be minimized. Of course, the optimization is expected to yield different results depending on the value assigned to w.

B. Constraints

As discussed in II.*A*, the first constraint relates to the maximum number of turns N_0 which can be accommodated around a wound tooth. The condition, expressed by (4) for the $k\text{th tooth}$, can be formulated compactly for all the teeth using the turn vector $\mathbf{x}$ as follows:

$$\mathbf{A}_1\mathbf{x} \le \mathbf{b}_1. \quad (67)$$

where $\mathbf{A}_1$ is the $Z \times 6Z$ matrix and $\mathbf{b}_1$ is the Z-sized vector below:

$$\mathbf{A}_1 = \begin{pmatrix} \mathbf{1}_{1\times 6} & \mathbf{0}_{1\times 6} & \cdots & \mathbf{0}_{1\times 6} \\ \mathbf{0}_{1\times 6} & \mathbf{1}_{1\times 6} & \cdots & \mathbf{0}_{1\times 6} \\ \vdots & \vdots & \ddots & \vdots \\ \mathbf{0}_{1\times 6} & \mathbf{0}_{1\times 6} & \cdots & \mathbf{1}_{1\times 6} \end{pmatrix},\ \mathbf{b}_1 = N_0\mathbf{1}_{Z\times 1} \quad (68)$$

with $\mathbf{1}_{m\times n}$ and $\mathbf{0}_{m\times n}$ indicating the $m \times n$ unit and zero matrix, respectively.

TABLE I
CHARACTERISTIC DATA OF THE EXAMPLE MACHINE

Number of stator slots, Z	9	Maximum number of turns per coil, N_0	100
Number of pole pairs, p	4	Peak value of stator current, I_0	8 A
Stator bore radius, R_s	55 mm	Stator frequency, f	50 Hz
Rotor core diameter R_r	48 mm	Magnet permeability, μ	$4\pi 10^{-7}$ H/ m
Permanent magnet height, h_m	4 mm	Magnet electrical conductivity, σ	0.667 MSm
Air gap width, g	3 mm	Magnet to pole span ratio, c_m	0.8
Core length, L	100 mm	Stator and rotor core permeability	$4\pi 10^{-2}$ H/ m

Moreover, according to the convention established in II.A, all the turn vector elements must be null or positive, i.e.,

$$\mathbf{A}_2\mathbf{x} \leq \mathbf{b}_2 \tag{69}$$

with $\mathbf{A}_2$ being the opposite of the $6Z \times 6Z$ identity matrix $\mathbf{I}_{6Z}$ and $\mathbf{b}_2$ the $6Z$-sized null vector:

$$\mathbf{A}_2 = -\mathbf{I}_{6Z},\ \mathbf{b}_2 = \mathbf{0}_{6Z\times 1} \tag{70}$$

The last constraint relates to the symmetry of the winding. For the winding to be symmetric, all the three phases must produce equal MMF fundamentals at any instant. In II.*C* it has been shown how this condition can be formalized with the following equation:

$$\mathbf{A}_3\mathbf{x} = \mathbf{b}_3 \tag{71}$$

where, based on (35), $\mathbf{A}_3$ and $\mathbf{b}_3$ are the $4 \times 6Z$ matrix and 4×1 vector below:

$$\mathbf{A}_3 = \begin{pmatrix} \mathrm{Re}\left\{v_p^{-T}\left(\mathbf{K}_b - \mathbf{K}_a\right)\right\} \\ \mathrm{Im}\left\{v_p^{-T}\left(\mathbf{K}_b - \mathbf{K}_a\right)\right\} \\ \mathrm{Re}\left\{v_p^{-T}\left(\mathbf{K}_c - \mathbf{K}_b\right)\right\} \\ \mathrm{Im}\left\{v_p^{-T}\left(\mathbf{K}_c - \mathbf{K}_b\right)\right\} \end{pmatrix},\ \mathbf{b}_3 = \begin{pmatrix} 0 \\ 0 \\ 0 \\ 0 \end{pmatrix}. \tag{72}$$

C. Problem Formulation and Interpretation of the Solution

In conclusion, the overall FSCW optimization problem can be formulated as follows:

$$\text{minimize } f_w(\mathbf{x}) \quad \text{subject to}$$
$$\begin{pmatrix} \mathbf{A}_1 \\ \mathbf{A}_2 \end{pmatrix}\mathbf{x} \leq \begin{pmatrix} \mathbf{b}_1 \\ \mathbf{b}_2 \end{pmatrix},\ \mathbf{A}_3\mathbf{x} = \mathbf{b}_3. \tag{73}$$

The solution of (73) gives an "optimal" turn vector $\mathbf{x}$ which defines a FSCW configuration like that shown in Fig. 1(b), with six sub-coils per tooth. More precisely, the number of turns $N_{k,j} \geq 0$ of the jth sub-coil wound on the kth tooth is automatically determined from (17) once the solution $\mathbf{x}$ is found. The physical design of interest is, of course, that shown in Fig. 1(a), with (at most) three phase coils per tooth. The number of turns (with sign) $N_{k,a}$, $N_{k,b}$ and $N_{k,c}$ for the three coils wound on the kth tooth can be determined by (6).

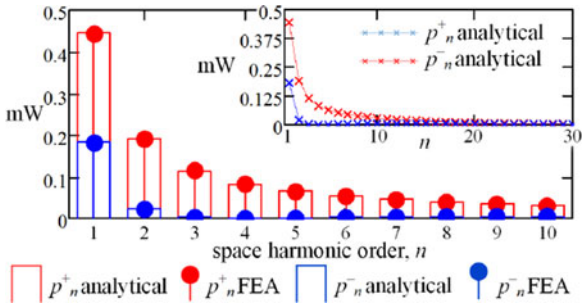

Fig. 6. Magnet losses produced by MMF harmonics (assumed of unit magnitude, 1 A) computed by (60) and by the FEA model shown in Fig. 7.

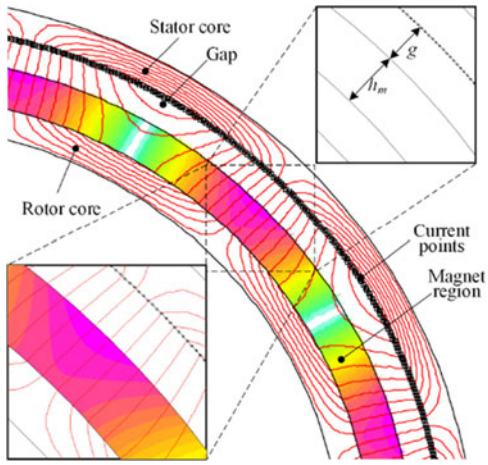

Fig. 7. Model to compute magnet losses due to a MMF harmonic through a time-harmonic FEA simulation.

TABLE II
WEIGHING COEFFICIENT VALUES FOR EIGHT DESIGNS

Design ID	#1	#2	#3	#4	#5	#6	#7	#8
Weighing factor w	0	.9997	.9998	.9999	.99992	.99993	.999935	.999944

V. APPLICATION EXAMPLE AND VALIDATIONS

An application example is illustrated for the proposed algorithm to the 9-slot 8-pole FSCW SPM machine characterized by the data listed in Table I.

As an application example, the quadratic programming problem (73) is implemented and solved in the MATLAB environment. The harmonic loss coefficients $p_n^{\pm}$ needed to define the matric $\mathbf{F}_w$ according to (66) are given in Fig. 6. Their analytically-computed value, resulting from (60), is compared to the value obtained by a time-harmonic FEA simulation. For this comparison, the generic MMF harmonic of order n having 1 A magnitude, associated to the rotor frequency $f(1 \pm n/p)$, is modeled as an equivalent sequence of equally-spaced current points distributed along the stator bore circumference [19]–[22] as depicted in Fig. 7. The magnet losses due to such harmonic are computed by running a time-harmonic FEA simulation at

TABLE III
NUMBER OF TURNS $N_{k,a}$, $N_{k,b}$, $N_{k,c}$ FOR THE EIGHT DESIGNS

		Tooth index k								
		$k=0$	$k=1$	$k=2$	$k=3$	$k=4$	$k=5$	$k=6$	$k=7$	$k=8$
design #1	$N_{k,a}$	0	0	100	−100	100	0	0	0	0
	$N_{k,b}$	0	0	0	0	0	100	−100	100	0
	$N_{k,c}$	−100	100	0	0	0	0	0	0	100
design #2	$N_{k,a}$	0	−50	100	−100	50	0	0	0	0
	$N_{k,b}$	0	0	0	0	−50	100	−100	50	0
	$N_{k,c}$	−100	50	0	0	0	0	0	−50	100
design #3	$N_{k,a}$	0	0	26.27	−73.73	100	−73.73	26.27	0	0
	$N_{k,b}$	26.27	0	0	0	0	26.27	−73.73	100	−73.73
	$N_{k,c}$	−73.73	100	−73.73	26.27	0	0	0	0	26.27
design #4	$N_{k,a}$	0	0	31.09	−68.91	100	−68.91	31.09	0	0
	$N_{k,b}$	31.09	0	0	0	0	31.09	−68.91	100	−68.91
	$N_{k,c}$	−68.91	100	−68.91	31.09	0	0	0	0	31.09
design #5	$N_{k,a}$	0	0	32.047	−67.95	100	−67.95	32.047	0	0
	$N_{k,b}$	32.05	0	0	0	0	32.047	−67.95	100	−67.953
	$N_{k,c}$	−67.95	100	−67.95	32.05	0	0	0	0	32.047
design #6	$N_{k,a}$	0	0	16.436	−50	83.564	−83.56	50	−16.44	0
	$N_{k,b}$	50	−16.44	0	0	0	16.436	−50	83.56	−83.564
	$N_{k,c}$	−50	83.564	−83.56	50	−16.44	0	0	0	16.436
design #7	$N_{k,a}$	16.94	−50	83.059	−83.06	50	−16.94	0	0	0
	$N_{k,b}$	0	0	0	16.94	−50	83.059	−83.06	50	−16.941
	$N_{k,c}$	−83.06	50	−16.94	0	0	0	16.941	−50	83.059
design #8	$N_{k,a}$	17.44	−50	82.556	−82.56	50	−17.44	0	0	0
	$N_{k,b}$	0	0	0	17.44	−50	82.556	−82.56	50	−17.444
	$N_{k,c}$	−82.56	50	−17.44	0	0	0	17.444	−50	82.556

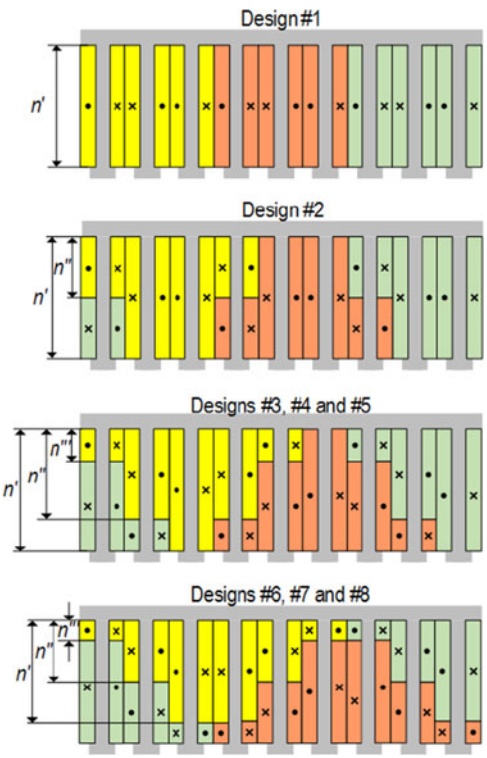

Fig. 8. FSCW design configurations resulting from the quadratic optimizations. Colors indicate different phases; symbols "•" and "×" indicate current conventional directions.

frequency $f(1 \pm n/p)$ [19]–[22]. Fig. 6. demonstrates a very good accordance between the loss coefficients predicted analytically and by FEA.

TABLE IV
CHARACTERISTIC NUMBERS OF TURNS FOR THE TOOTH COILS

	Design ID							
	#1	#2	#3	#4	#5	#6	#7	#8
n'/N_0	1.0000	1.0000	1.0000	1.0000	1.0000	0.8356	0.8306	0.8256
n''/N_0	–	0.5000	0.2627	0.3109	0.3205	0.5000	0.5000	0.5000
n'''/N_0	–	–	0.7373	0.6891	0.6795	0.1644	0.1694	0.1744

The quadratic programming problem (73) is solved for the eight different values of the weight w given in Table II, obtaining the eight corresponding FSCW designs designated as #1, #2, . . . , #8.

The optimization output for all the eight designs is summarized in Table III in terms of the number of turns per phase wound around each stator tooth (Fig. 1(a)).

For better clarity, the FSCW arrangements corresponding to the eight optimal designs are visualized in Fig. 8. The characteristic sizes (or numbers of turns n', n'', n''') for the various unequal coils are detailed in Table IV.

Fig. 8 shows that the design #1, obtained setting $w = 0$, is the standard dual-layer configuration which is given by the star-of-slots method [10]. In fact, setting $w = 0$ means that the optimization tends to maximize the MMF fundamental with no regard to magnet losses and the star-of-slots method appears to yield the optimal choice for this purpose. In this sense, it is clear that, with the position $w = 0$, the proposed algorithm "degenerates" into the star-of-slot method and does not give any more information than it. Conversely, as the weight w increases

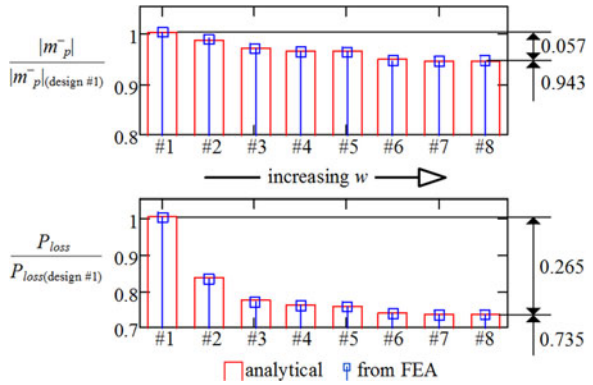

Fig. 9. Fundamental MMF magnitude and magnet loss for the eight designs #1, #2, ..., #8 in per unit of their value for the standard FSCW configuration (design #1).

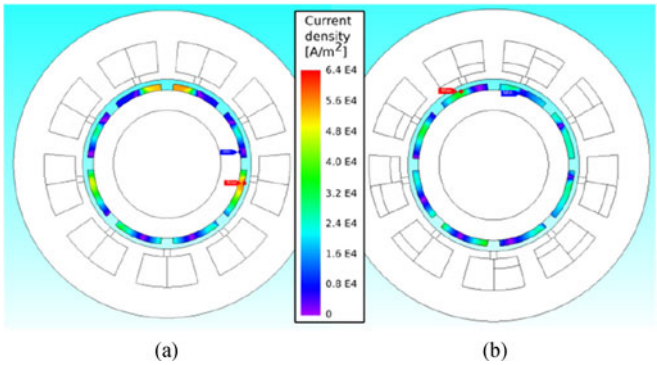

Fig. 10. Examples of magnet loss computation by time-stepping FEA: (a) for design #1; (b) for design #5. Current density maps are represented with the same color scale, showing larger losses in the case of design #1. Fig. 10. Model used for FEA simulations.

towards 1, the magnet loss minimization is given more and more importance at the expense of MMF fundamental magnitude as per (66). The resulting designs are then expected to have decreasing magnet losses and, at the same time, decreasing MMF fundamental amplitudes. This is confirmed if we look at Fig. 9: when we pass from the standard dual-layer FSCW configuration (design #1) to design #8, the MMF fundamental reduces by 5.7% and magnet losses reduce by 26.5%. Both reductions are monotonic.

Incidentally, the MMF fundamental amplitudes and magnet losses obtained analytically from (20) and (62) are compared in Fig. 9. to the values resulting from FEA. For this purpose, the model shown in Fig. 10. is implemented in JMAG 16.0. Time-stepping FEA simulations are run in order to compute magnet losses at steady state; magnetostatic simulations are, instead, run to obtain the radial flux density B_r profile along the mean air-gap circumference and, from this, to estimate the air-gap MMF as $B_r(g + h_m)/\mu_0$. It can be seen that a good accordance between FEA and analytical results is obtained for both MMF and magnet loss prediction. The same FEA simulations are used to assess the perfect symmetry of all the winding designs.

Looking at Fig. 8. it appears that magnet loss reduction is achieved, at the expense of a lowered MMF fundamental, paying the toll of an increasing winding complexity as summarized in

TABLE V
CHARACTERISTIC NUMBERS OF TURNS FOR THE TOOTH COILS

	Design ID							
	#1	#2	#3	#4	#5	#6	#7	#8
Number of layers	2	2 or 3	3 or 4	3 or 4	3 or 4	4	4	4
Number of different coil sizes	1	2	3	3	3	3	3	3

Table V. The increasing complexity is due to the growth in the number of layers and different coil sizes to be included in the winding design.

It is noticed that the hybrid two/three layer structure of design #2 is the same as that obtained in [10] from a four-layer layout by merging two identical coils of the same phase wound around the same tooth.

Regarding designs #3, #4 and #5, their structure is substantially the same as the "optimal" configuration presented in [15], where the ratio $n''/n''' = 2$ is proposed to obtain the cancellation of the first-order MMF harmonic.

As a result of the optimization approach herein adopted, however, it is observed that the structure of designs #3, #4 and #5 cannot be identified as "optimal" from a rotor loss minimization viewpoint. In fact, it can be further enhanced using the layout of designs #6, #7 and #8, where two coils of different phases (with either equal or unequal size) are wound around each tooth. This layout has been never reported in the previous literature, to the author's knowledge, and seems to represent the best solution for the 9-slot 8-pole FSCW example taken into account in terms of rotor loss minimization. This is deduced from the fact that increasing the weight coefficient w above 0.999944 (i.e., the value giving design #8 as per Table II) causes the quadratic optimization problem (73) to result in the null solution $\mathbf{x} = \mathbf{0}_{54\times 1}$. Such null solution is obviously feasible and such to minimize magnet losses ($P_{loss} = 0$) but is not practically interesting as it also implies a zero MMF fundamental. In other words, it is reasonable to assume that the 9-slot 8-pole configuration of practical interest leading to minimal rotor losses is the one characterizing designs #6, #7 and #8, i.e., with three coil sizes respectively including (more or less) 17%, 50% and 83% (Table IV) of the total number of turns N_0 that can be wound around a single tooth.

Finally, a short insight is next provided into the way how the proposed optimization algorithm automatically achieves the optimal solution for any given weight coefficient w. This can be understood looking at the MMF harmonic content (Figs. 11 and 12) of the eight designs #1, #2, ..., #8 obtained for increasing values of w. In addition to the fundamental (m_4^-), there are various MMF harmonics with relatively large amplitudes. However, it can be seen that, in the attempt to minimize rotor losses, the algorithm acts differently on the various harmonics. For instance, the harmonics with orders 13, 14, 22 and 23, although large, are only slightly reduced as they are associated to very small loss coefficients (p_{13}^-, p_{13}^-, p_{14}^+, p_{22}^-, and p_{23}^+ in Fig. 6). Conversely, the subharmonics (of orders 1 and 2) are significantly abated for

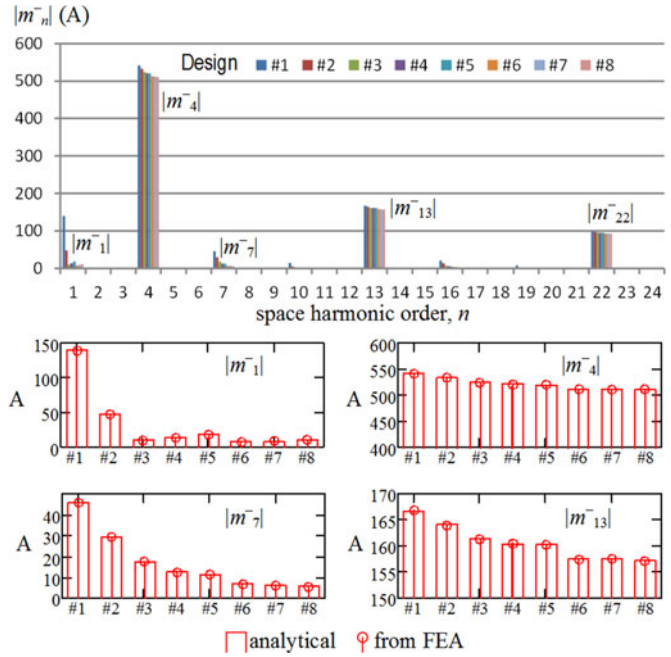

Fig. 11. Magnitude of MMF harmonics revolving in the same direction as the rotor for the eight designs #1, #2, . . . , #8.

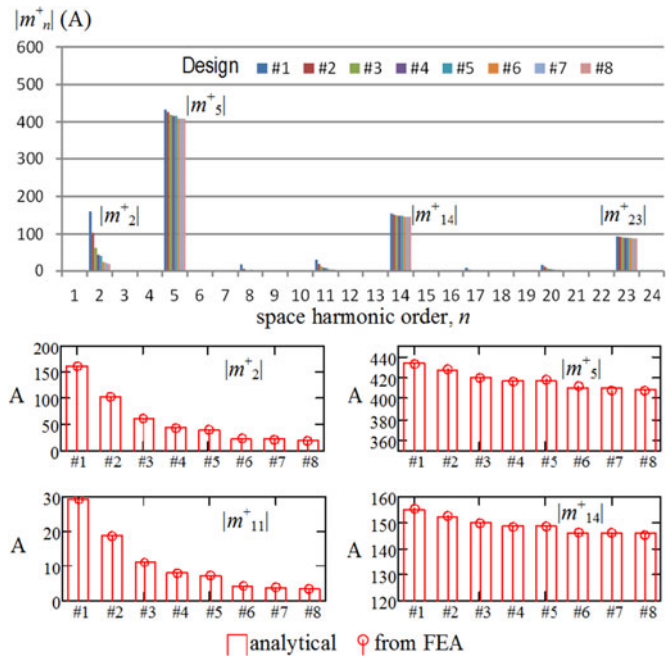

Fig. 12. Magnitude of counter-rotating MMF harmonics for the eight designs #1, #2, . . . , #8.

growing w because they are associated to large magnet loss coefficients (p_1^- and p_2^+ in Fig. 6). It is also important to observe how the algorithm does not act on a given subharmonic separately. For example, no optimal solution is found for which either the first- or second-order subharmonic is canceled. Differently from what is usually done in the literature, in fact, the minimization of the total rotor losses is the goal instead of the cancellation of a single subharmonic. For instance, Figs. 11 and 12 show that, while the second-order subharmonic monotonically decreases with w, the first harmonic does not: more precisely, it is reduced when passing from design #1 to #2, from #2 to #3 and from #5 to #6 (i.e., when transitioning between the four winding layouts shown in Fig. 6), while it slightly increases in the transitions from designs #3 to #4, #4 to #5, #6 to #7 and #7 to #8. Evidently, the strength of the proposed algorithm is, among the other things, the capability of automatically identifying which harmonics are to be increased and which are to be decreased – and to what extent – in order for the total rotor losses to be reduced.

VI. Conclusion

In addition to various attractive features, the use of a FSCW for synchronous permanent magnet machines has the drawback of causing large air-gap MMF harmonics and consequent rotor losses. It is already known that increasing the number of layers and also using coils with different number of turns can be beneficial for reducing FSCW harmonics. So far, however, FSCW design optimization has been approached on a case-by-case basis and finding the optimum, though extensive theoretical or heuristic reasoning, for any individual slot/pole combination. In this paper a new general and systematic methodology has been proposed to optimize the FSCW of a three-phase SPM machine through the numerical solution of a quadratic programming problem. Although requiring a certain theoretical effort for their derivation, the final matrices used to formulate the quadratic programming problem has a very simple easy-to-compute expression for any slot/pole combination and any SPM machine geometry. Two objective functions (fundamental MMF maximization and rotor loss minimization) are incorporated in the problem and given more or less relative importance through the choice of a weighing coefficient. For any weight selection, the algorithm outputs the best design automatically identifying the optimal number of layers, the optimal number of turns for each coil and the optimal assignment of the coils to the phases, without requiring any reasoning or intervention by the designer and guaranteeing winding symmetry and feasibility. Differently from what is usually done, the proposed algorithm does not aim at cancelling a specific MMF harmonic but tends to minimize the overall rotor losses, automatically determining which space harmonics, and to what extent, need to be adjusted for that purpose. An application example has been reported to a 9-slot 8-pole SPM machine and extensive FEA simulations have been presented for validation. Among the other things, it has been shown that the proposed algorithm, depending on how the objective functions are weighed, can output various optimal design configurations: some of these are known from the literature as the result of previous dedicated optimizations, other ones are original and proved to yield a further improvement.

The proposed methodology is intrinsically suitable for extension to a generic m-phase winding, with m different from 3, through only formal modifications to the treatment included in the paper.

In conclusion, the proposed approach is found to include all the features of the star-of-slot method, while enriching them

with new additional optimization potentials. It is therefore envisioned as a new promising tool for a fully-automated and more comprehensive FSCW design optimization.

REFERENCES

[1] A.M. El-Refaie, "Fractional-slot concentrated-windings synchronous permanent magnet machines: Opportunities and challenges," *IEEE Trans. Ind. Electron.*, vol. 57, no. 1, pp. 107–121, Jan. 2010.

[2] A. Tessarolo, F. Luise, S. Pieri, A. Benedetti, M. Bortolozzi, and M. De Martin, "Design for manufacturability of an Off-Shore Direct-Drive wind generator: An insight into additional loss prediction and mitigation," *IEEE Trans. Ind. Appl.*, to be published.

[3] A. M. El-Refaie and T. M. Jahns, "Scalability of surface PM Machines with concentrated windings designed to achieve wide speed ranges of constant-power operation," *IEEE Trans. Energy Convers.*, vol. 21, no. 2, pp. 362–369, Jun. 2006.

[4] E. Fornasiero, L. Alberti, N. Bianchi, and S. Bolognani, "Considerations on selecting fractional-slot nonoverlapped coil windings," *IEEE Trans. Ind. Appl.*, vol. 49, no. 3, pp. 1316–1324, May/Jun. 2013.

[5] C. M. Spargo, B. C. Mecrow, J. D. Widmer, C. Morton, and N. J. Baker, "Design and validation of a synchronous reluctance motor with single tooth windings," *IEEE Trans. Energy Convers.*, vol. 30, no. 2, pp. 795–805, Jun. 2015.

[6] N. Bianchi and E. Fornasiero, "Impact of MMF space harmonic on rotor losses in fractional-slot Permanent-Magnet machines," *IEEE Trans. Energy Convers.*, vol. 24, no. 2, pp. 323–328, Jun. 2009.

[7] A. Tessarolo, "A survey of state-of-the-art methods to compute rotor eddy-current losses in synchronous permanent magnet machines," in *Proc. IEEE Workshop Elect. Mach. Design, Control Diagnosis*, Nottingham, United Kingdom, 2017, pp. 12–19.

[8] A. S. Abdel-Khalik, S. Ahmed, and A. M. Massoud, "Low space harmonics cancelation in Double-Layer fractional slot winding using dual multiphase winding," *IEEE Trans. Magn.*, vol. 51, no. 5, May 2015, Art. no. 8104710.

[9] A. S. Abdel-Khalik, S. Ahmed, and A. M. Massoud, "Low space harmonics cancelation in Double-Layer fractional slot winding using dual multiphase winding," *IEEE Trans. Magn.*, vol. 51, no. 5, May 2015, Art. no. 8104710.

[10] L. Alberti and N. Bianchi, "Theory and design of Fractional-Slot multilayer windings," *IEEE Trans. Ind. Appl.*, vol. 49, no. 2, pp. 841–849, Mar./Apr. 2013.

[11] Y. Wang, R. Qu, and J. Li, "Multilayer windings effect on interior PM machines for EV applications," in *IEEE Trans. Ind. Appl.*, vol. 51, no. 3, pp. 2208–2215, May/Jun. 2015.

[12] A. Sun, J. Li, R. Qu, and D. Li, "Effect of multilayer windings on rotor losses of interior permanent magnet generator with Fractional-Slot Concentrated-Windings," *IEEE Trans. Magn.*, vol. 50, no. 11, Nov. 2014, Art. no. 8105404.

[13] Y. Wang, R. Qu, and J. Li, "Multilayer windings effect on interior PM machines for EV applications," in *IEEE Trans. Ind. Appl.*, vol. 51, no. 3, pp. 2208–2215, May/Jun. 2015.

[14] D. Gerlando, A. Perini, and M. R. Ubaldini, "High pole number, PM synchronous motors with concentrated coil armature winding," in *Proc. Int. Conf. Electr. Mach.*, Krakow, Poland, 2004, pp. 307–320.

[15] M. V. Cistelecan, F. J. T. E. Ferreira, and M. Popescu, "Three phase tooth concentrated multiple-layer fractional windings with low space harmonic content," in *Proc. IEEE Energy Convers. Congr. Expo.*, 2010, pp. 1399–1405.

[16] L. Alberti, M. Barcaro, and N. Bianchi, "Design of a Low-Torque-ripple fractional-slot interior permanent-magnet motor," *IEEE Trans. Ind. Appl.*, vol. 50, no. 3, pp. 1801–1808, May/Jun. 2014.

[17] A. Tessarolo, M. Mezzarobba, and N. Barbini, "Improved four-layer winding design for a 12-slot 10-pole permanent magnet machine using unequal tooth coils," in *Proc. IEEE IECON 2016 - 42nd Annual Conf. Ind. Electron. Soc.*, Florence, 2016, pp. 1686–1691.

[18] T.F. Coleman and Y. Li, "A reflective newton method for minimizing a quadratic function subject to bounds on some of the variables," *SIAM J. Optimization*, vol. 6, no. 4, pp. 1040–1058, 1996.

[19] F. Luise, S. Pieri, M. Mezzarobba, and A. Tessarolo, "Regenerative testing of a Concentrated-Winding Permanent-Magnet synchronous machine for offshore wind generation—Part I: Test concept and analysis," *IEEE Trans. Ind. Appl.*, vol. 48, no. 6, pp. 1779–1790, Nov./Dec. 2012.

[20] M. Olivo, A. Tessarolo, and M. Bortolozzi, "On the use of conformai mapping in the analysis of electric machines," in *Proc. 2016 XXII Int. Conf. Elect. Mach.*, Lausanne, 2016, pp. 492–498.

[21] P. Arumugam, T. Hamiti, and C. Gerada, "Estimation of eddy current loss in Semi-Closed slot vertical conductor permanent magnet synchronous machines considering eddy current reaction effect," *IEEE Trans. Magn.*, vol. 49, no. 10, pp. 5326–5335, Oct. 2013.

[22] N. Bianchi, S. Bolognani, and E. Fornasiero, "An overview of rotor losses determination in Three-Phase Fractional-Slot PM machines," *IEEE Trans. Ind. Appl.*, vol. 46, no. 6, pp. 2338–2345, Nov./Dec. 2010.

Alberto Tessarolo received the Laurea and Ph.D. degrees in electrical engineering from the University of Trieste, Trieste, Italy, in 2000 and 2011, respectively. Before joining the University, he worked in the design and development of large innovative motors, generators and drives with NIDEC-ASI (formerly Ansaldo Sistemi Industriali). Since 2006, he has been with the Department of Engineering and Architecture, University of Trieste, where he teaches the course of Electric Machine Design. He holds the scientific responsibility for several funded research projects in cooperation with leading companies and institutions. He has authored more than 150 international technical papers in the area of electrical machine and drive modeling and design. He serves as an Editor for the IEEE TRANSACTIONS ON ENERGY CONVERSION and Associate Editor for the IEEE TRANSACTIONS ON INDUSTRY APPLICATIONS and *IET Electric Power Applications*. He received the Electric Machinery Committee 2012 Prize Paper Award of the IEEE Power and Energy Society and of various best paper awards for contributions presented at IEEE-sponsored or co-sponsored conferences. He is a senior member of the IEEE and a member of the Industry Applications, Power and Energy, Power Electronics, Industrial Electronics, and Magnetics and Reliability Societies of the IEEE.